

University of Nebraska - Lincoln

DigitalCommons@University of Nebraska - Lincoln

Vadim Gladyshev Publications

Biochemistry, Department of

May 2007

Crystal Structure of Formate Dehydrogenase H: Catalysis Involving Mo, Molybdopterin, Selenocysteine, and an Fe₄S₄ Cluster

Jeffrey C. Boyington
National Institutes of Health (NIH), Rockville, MD


Vadim Gladyshev
University of Nebraska-Lincoln, vgladyshev@rics.bwh.harvard.edu

Sergei V. Khangulov
Princeton University, Princeton, NJ

Thressa C. Stadtman
National Institutes of Health (NIH), Rockville, MD

Peter D. Sun
National Institutes of Health (NIH), Rockville, MD

Follow this and additional works at: <https://digitalcommons.unl.edu/biochemgladyshev>

 Part of the [Biochemistry, Biophysics, and Structural Biology Commons](#)

Boyington, Jeffrey C.; Gladyshev, Vadim; Khangulov, Sergei V.; Stadtman, Thressa C.; and Sun, Peter D., "Crystal Structure of Formate Dehydrogenase H: Catalysis Involving Mo, Molybdopterin, Selenocysteine, and an Fe₄S₄ Cluster" (2007). *Vadim Gladyshev Publications*. 29.

<https://digitalcommons.unl.edu/biochemgladyshev/29>

This Article is brought to you for free and open access by the Biochemistry, Department of at DigitalCommons@University of Nebraska - Lincoln. It has been accepted for inclusion in Vadim Gladyshev Publications by an authorized administrator of DigitalCommons@University of Nebraska - Lincoln.

Crystal Structure of Formate Dehydrogenase H: Catalysis Involving Mo, Molybdopterin, Selenocysteine, and an Fe₄S₄ Cluster

Jeffrey C. Boyington, Vadim N. Gladyshev,*
Sergei V. Khangulov, Thressa C. Stadtman, Peter D. Sun†

Formate dehydrogenase H from *Escherichia coli* contains selenocysteine (SeCys), molybdenum, two molybdopterin guanine dinucleotide (MGD) cofactors, and an Fe₄S₄ cluster at the active site and catalyzes the two-electron oxidation of formate to carbon dioxide. The crystal structures of the oxidized [Mo(VI), Fe₄S_{4(ox)}] form of formate dehydrogenase H (with and without bound inhibitor) and the reduced [Mo(IV), Fe₄S_{4(red)}] form have been determined, revealing a four-domain $\alpha\beta$ structure with the molybdenum directly coordinated to selenium and both MGD cofactors. These structures suggest a reaction mechanism that directly involves SeCys¹⁴⁰ and His¹⁴¹ in proton abstraction and the molybdenum, molybdopterin, Lys⁴⁴, and the Fe₄S₄ cluster in electron transfer.

Formate dehydrogenase H (FDH_H), a 79-kD polypeptide that oxidizes formate to carbon dioxide with the release of a proton and two electrons, is a component of the anaerobic formate hydrogen lyase complex of *E. coli* (1). Essential to its catalytic activity are an Fe₄S₄ cluster, a Mo atom that is coordinated by two MGD cofactors, and a SeCys residue (2–4). With the recent determination of the crystal structures of three other molybdopterin (MPT)–containing enzymes (5–8), a functional role for the Mo–MPT cofactor has begun to emerge. However, the precise role of the active site selenium in this type of selenoenzyme and its interaction with Mo–MPT cofactors and the Fe₄S₄ cluster remains to be elucidated (9).

The structure of *E. coli* FDH_H, as solved by multiple isomorphous replacement (MIR) and multiwavelength anomalous dispersion (MAD) methods (Table 1), consists of four $\alpha\beta$ domains (Fig. 1). The first domain (residues 1 to 60, 448 to 476, and 499 to 540), comprising two small antiparallel β sheets and four helices, coordinates the Fe₄S₄ cluster just below the protein surface. The MGD-binding domains II (residues 61 to 135, 336 to 447, and 477 to 498) and III (residues 136 to 335) are each $\alpha\beta\alpha$ sandwiches with overall topologies that closely resemble the classical dinucleotide-binding fold (10). A marked twofold pseudosymmetry is observed relating the cen-

tral portions of domains II and III. Despite their low sequence homology (<20% identity), the two domains can be superimposed to a root-mean-square (rms) deviation of 1.2 Å for 56 α carbons. SeCys¹⁴⁰, an essential ligand to Mo, is located in a short loop at the NH₂-terminus of domain III. The COOH-terminal domain (residues 541 to 715) consists of a

six-stranded mixed β barrel and five helices.

Similar to the active sites observed in aldehyde ferredoxin oxidoreductase and dimethyl sulfoxide (DMSO) reductase, the active site Mo of FDH_H is coordinated by two tightly bound MGD cofactors, each containing a tricyclic ring system with a pyran ring fused to the pterin (6, 7). The Mo di(MGD) of FDH_H is ligated within the interfaces of all four domains through an extensive network of hydrogen bonds, salt bridges, and van der Waals interactions, most of which involve domains II, III, and IV (Fig. 2). Domain II exclusively coordinates MGD⁸⁰¹ while domain III coordinates MGD⁸⁰². Domain IV forms a cap over the bound pterin cofactors as it straddles domains II and III. Of the 35 residues that coordinate the Mo di(MGD) cofactor through hydrogen bonds, 23 are well conserved among the known MGD-containing formate dehydrogenases (11); the remaining 12 residues interact primarily through main chain hydrogen bonds (Fig. 2).

In both the reduced Mo(IV) and oxidized Mo(VI) structures, Mo is ligated to the four cis-dithiolene sulfurs of the MGD cofactors and the selenium of SeCys¹⁴⁰. The coordination geometry of Mo in formate-reduced FDH_H is closely approximated by a square

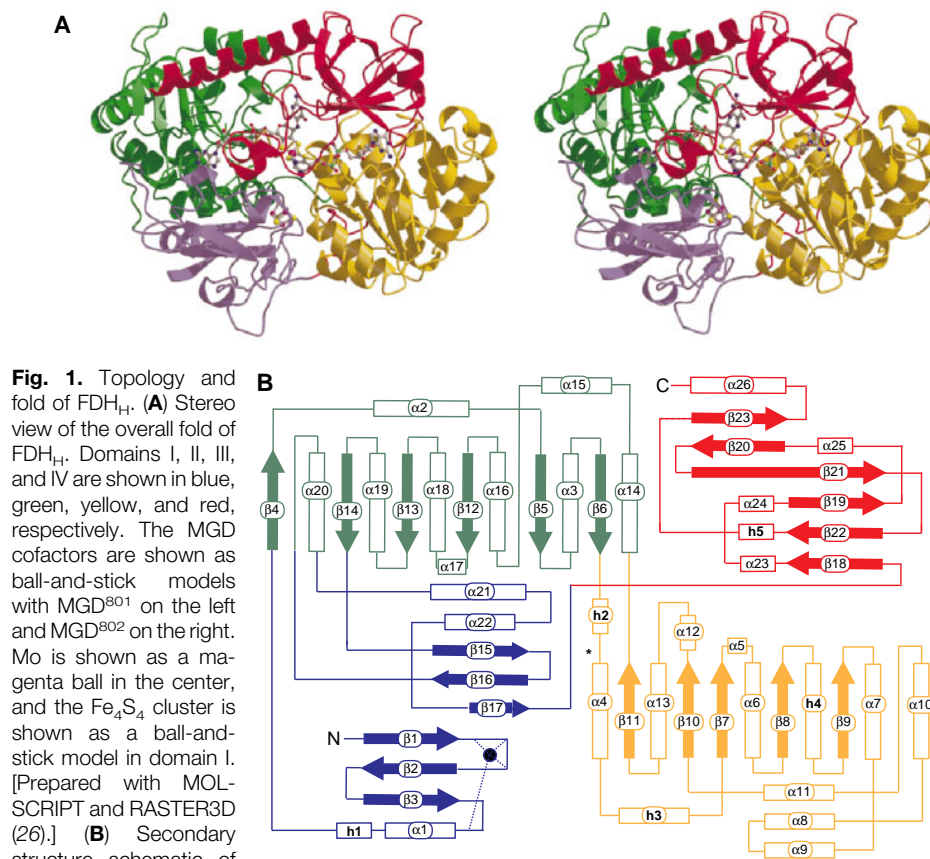


Fig. 1. Topology and fold of FDH_H. (A) Stereo view of the overall fold of FDH_H. Domains I, II, III, and IV are shown in blue, green, yellow, and red, respectively. The MGD cofactors are shown as ball-and-stick models with MGD⁸⁰¹ on the left and MGD⁸⁰² on the right. Mo is shown as a magenta ball in the center, and the Fe₄S₄ cluster is shown as a ball-and-stick model in domain I. [Prepared with MOLSCRIPT and RASTER3D (26).] (B) Secondary structure schematic of FDH_H. Domains I to IV are color-coded as in (A); α helices are numbered from α 1 to α 26, 3₁₀ helices are numbered from h1 to h4, and β strands are numbered from β 1 to β 23. The location of SeCys¹⁴⁰ is denoted by an asterisk; the location of the Fe₄S₄ cluster is denoted by a solid blue circle.

J. C. Boyington and P. D. Sun, Structural Biology Section, Laboratory of Molecular Structure, National Institute of Allergy and Infectious Diseases, National Institutes of Health (NIH), 12441 Parklawn Drive, Rockville, MD 20852, USA.

V. N. Gladyshev and T. C. Stadtman, Laboratory of Biochemistry, National Heart, Lung, and Blood Institute, NIH, 9000 Rockville Pike, Bethesda, MD 20892, USA.

S. V. Khangulov, Department of Chemistry, Hoyt Laboratory, Princeton University, Princeton, NJ 08544, USA.

*Present address: Basic Research Laboratory, National Cancer Institute, NIH, 9000 Rockville Pike, Bethesda, MD 20892, USA.

†To whom correspondence should be addressed.

pyramid in which the sulfur atoms provide the four equatorial ligands and the selenium provides an axial ligand (Fig. 3) (12). The Mo atom is ~ 0.4 Å above the equatorial plane in the direction of the selenium. Upon oxidation of Mo(IV) to Mo(VI), however, the pterin portion of MGD⁸⁰¹ is rotated 27° away from the equatorial plane and 16° along its own long axis. In contrast, little movement is observed in MGD⁸⁰² or in the guanine nucleotide portion of MGD⁸⁰¹. The fifth ligand, the selenium atom of SeCys¹⁴⁰, moves 0.9 Å closer to S12 of MGD⁸⁰², resulting in a slightly longer bond to Mo (2.7 Å). The four sulfur ligand distances to Mo also increase slightly (to between 2.3 and 2.6 Å) in the oxidized state (12). $F_{\text{obs}} - F_{\text{calc}}$ electron density maps revealed the presence of a sixth ligand in the Mo(VI) state, giving the Mo a trigonal prismatic coordination geometry (Fig. 3). This ligand was modeled as a hydroxyl group that refined to a distance of 2.2 Å from Mo with a B factor of 16.8 Å². The position of the SeCys¹⁴⁰ β carbon in the oxidized state also

enables a new water molecule, H₂O⁶⁴, to interact with the amide of His¹⁴¹ and the NH1 of Arg³³³, whose side chain moves 3.9 Å toward H₂O⁶⁴. Redox-induced conformational changes result in minor domain movements and minor alterations in the hydrogen-bonding network coordinating MGD⁸⁰¹ (Fig. 2).

The binding of the nitrite inhibitor (2, 3) to the oxidized FDH_H is clearly visible in the initial $F_{\text{obs}} - F_{\text{calc}}$ electron density map as a crescent-shaped 4σ peak indicating displacement of the hydroxyl ligand originally at the same position (Fig. 4). One nitrite oxygen is bound to the Mo (bond length 2.5 Å); the other is hydrogen-bonded to both the main chain amide of His¹⁴¹ and the side chain of Arg³³³, which moves 0.5 Å closer to Mo in order to accommodate this hydrogen bond. Nitrite also displaces the H₂O⁶⁴ observed in oxidized FDH_H. Both Arg³³³ and His¹⁴¹ are strictly conserved in all Mo-dependent formate dehydrogenases (11). Apart from the nitrite-binding site, the structure of inhibitor-complexed oxidized FDH_H is essentially the

same as that of the benzyl viologen-oxidized enzyme. When formate is modeled into the nitrite-binding site, the α proton of formate is located less than 1.5 Å from the selenium of SeCys¹⁴⁰, poisoning it for abstraction by selenium. The side chain of His¹⁴¹ is positioned on the other side of the selenium, opposite the formate. This putative substrate-binding site lies at the bottom of a deep crevice located between domains II and III, with Arg³³³ at the base of the crevice providing both a positive charge and a critical hydrogen bond for orienting the substrate for catalysis.

Kinetic experiments have suggested that the two electrons from oxidized formate leave the enzyme one at a time through a ping-pong mechanism (3). The Fe₄S₄ cluster located just below the protein surface in domain I provides a one-electron sink for a downstream electron acceptor. The observed reduction of the Fe₄S₄ cluster upon substrate binding indicates that electrons must travel from the Mo center to the Fe₄S₄ cluster. The most direct path between the Mo atom and the Fe₄S₄ cluster is through the partially conjugated ring system of MGD⁸⁰², exiting through N20 and following the hydrogen bond pathway from H₂O³⁰ to the Nζ of Lys⁴⁴ to the S1 of the Fe₄S₄ cluster (Fig. 5). Both H₂O³⁰ and the Nζ of Lys⁴⁴ have well-ordered electron densities with temperature factors in the reduced form of 21.7 and 27.9 Å², respectively. Lys⁴⁴, although strictly conserved in the family of MGD-containing formate dehydrogenases (11), is completely buried in the interior of the protein and has no countercharge partner with which to interact.

Catalysis begins with formate replacing the Mo-bound hydroxyl in the [Mo(VI), Fe₄S_{4(ox)}] state of the enzyme, presumably

Fig. 2. Schematic representation of the hydrogen-bonding network coordinating MGD⁸⁰¹ and MGD⁸⁰². Residues are color-coded according to sequence conservation among the known sequences of MGD-containing FDH enzymes (11): magenta, invariant; blue, well conserved; and green, not conserved. The eight water molecules involved in hydrogen-bonding interactions are designated by orange circles. Hydrogen bonds present in the oxidized state, the reduced state, or both states are represented by blue, red, or black dashed lines, respectively. The binding of both MGD cofactors resembles the dinucleotide binding observed in the classical dinucleotide-binding proteins (10).

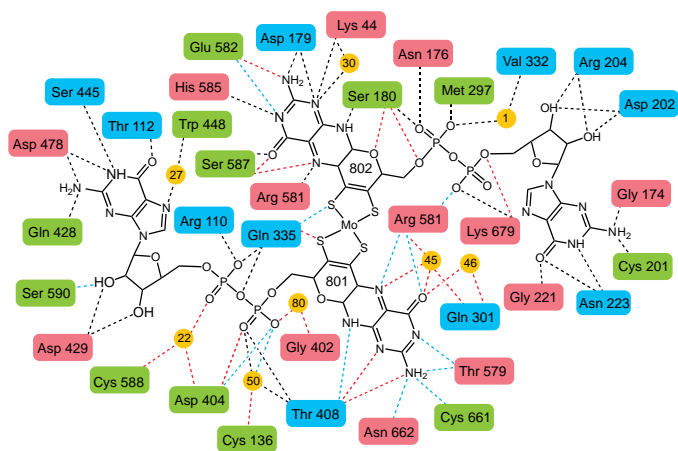


Fig. 3 (left). Superposition of the Mo center of FDH_H in the reduced [Mo(IV)] state (red) and oxidized [Mo(VI)] state (green). The Mo center (magenta) includes the active site residues SeCys¹⁴⁰, His¹⁴¹, and Arg³³³ and the pterin portions (MPT) of the Mo cofactors. [Prepared with MOLSCRIPT and RASTER3D (26).]

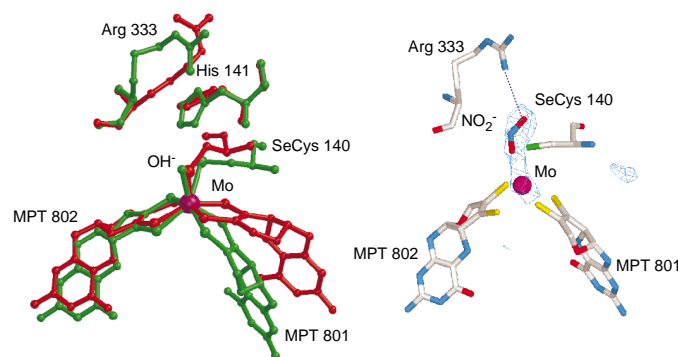


Fig. 4 (right). The nitrite-binding site. A 4σ $F_{\text{obs}} - F_{\text{calc}}$ electron density map calculated to 2.9 Å using phases from the uncomplexed oxidized FDH_H reveals the binding of the inhibitor nitrite. [Prepared with SETOR (27).] The coordinates for the reduced, oxidized, and nitrite-bound forms of FDH_H have been deposited in the Protein Data Bank (accession numbers 1aa6, 1fd0, and 1fdi, respectively).

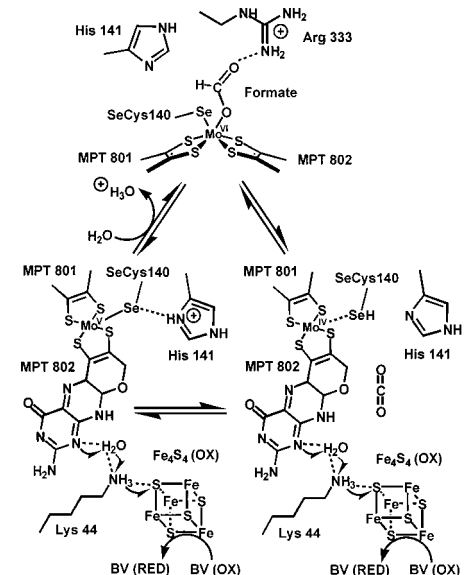


Fig. 5. The proposed reaction mechanism for FDH_H. BV, benzyl viologen.

being stabilized and oriented by hydrogen bonding through a carbonyl oxygen of formate to both Arg³³³ and the amide nitrogen of His¹⁴¹ (Fig. 5). The subsequent oxidation of formate to carbon dioxide and the transfer of two electrons to the Mo center (Fig. 5) may occur either by a direct two-electron transfer through the oxygen of formate to Mo or by a direct hydride transfer to Mo. Upon Mo reduction, the α proton of formate is released to the nearby His¹⁴¹ through protonation of SeCys¹⁴⁰. The involvement of a histidine residue is consistent with known pH dependencies in the catalytic activity of both the SeCys¹⁴⁰ \rightarrow Cys¹⁴⁰ mutant and wild-type FDH_H (13), and the protonation of His¹⁴¹ by the α proton of formate is supported by electron paramagnetic resonance (EPR) observations (14). The next step is to shuttle electrons from the Mo(IV) to a downstream electron acceptor through the

Fe₄S₄ cluster. As the first electron is transferred through Lys⁴⁴ to the Fe₄S₄ cluster, it produces an intermediate [Mo(V), Fe₄S₄(red)] that is easily observed in EPR experiments (14). Meanwhile, the transfer of a formate-derived proton to His¹⁴¹ will lead to hydrogen bond formation between the imidazole of His¹⁴¹ and the selenium of SeCys¹⁴⁰ while the selenium is coordinated to Mo(V) (15). Although the nature of the in vivo electron acceptor for FDH_H remains unknown, the reoxidation of the Fe₄S₄ can be achieved with benzyl viologen, a one-electron acceptor. Once the Fe₄S₄ cluster is reoxidized, a second electron can be transferred from Mo(V) to the Fe₄S₄ cluster and the enzyme returns to its initial state after the second oxidation of the Fe₄S₄ cluster. The oxidation of Mo(V) to Mo(VI) would cause the hydrogen bond between SeCys¹⁴⁰ and His¹⁴¹ to break, thereby re-

leasing the proton of His¹⁴¹ to solvent.

A common feature among many MPT-containing enzymes is the coupling of the redox state of Mo with the substrate oxidation-reduction process. In FDH_H, the reduction of Mo(VI) to Mo(IV) profoundly affects the Mo coordination geometry and thus the conformation of MPTs. Such changes, which are also observed in model compounds (16), may represent a general feature associated with MPT-dependent Mo- and W-containing enzymes. In contrast, the incorporation of a SeCys in FDH_H, as compared with incorporation of a Cys or Ser in other di(MPT)-dependent enzymes, appears to correlate with the usage of a hydroxyl ligand as opposed to sulfido or oxo ligands to Mo (7, 17, 18). This is also evident in extended x-ray absorption fine structure (EXAFS) studies of FDH_H where a terminal oxo ligand to Mo is observed in a SeCys¹⁴⁰ \rightarrow Cys¹⁴⁰ mutant but not in wild-type FDH_H (19). This mutation results in a much lower initial rate of substrate oxidation, 1/300 that of the wild type (13). Thus, the choice of a SeCys, Cys, or Ser ligand to Mo may serve to fine-tune the coordination of a particular cis-ligand and hence set the substrate preference. This suggests a new role of selenium in biology, involving ligation to a metal and proton transfer during catalysis.

The combination of the MPT redox center, SeCys¹⁴⁰, and the Fe₄S₄ cluster, each precisely positioned, results in an enzyme that not only catalyzes the oxidation of formate but also effectively couples the oxidation-reduction to an electron acceptor in the formate hydrogen lyase complex. This suggests that the MPT moiety, in addition to providing a structural framework for Mo coordination, also functions as part of an electron transfer path and potentially as an electron sink.

Table 1. Data collection, phasing, and refinement statistics for FDH_H structure determination. Purification, crystallization, and cryofreezing of reduced FDH_H crystals [Mo(IV), Fe₄S₄(red)] were performed in a nitrogen atmosphere at <1 ppm of oxygen as described (20). Crystals belong to the tetragonal space group *P*4₁2₁2 with cell dimensions of *a* = *b* = 146.3 Å and *c* = 82.3 Å containing one monomer in the asymmetric unit. Crystals of FDH_H in the [Mo(VI), Fe₄S₄(ox)] state (10) were obtained by serially washing crystals in a formate-free solution and then soaking crystals in 10 mM benzyl viologen for 30 min before freezing. Crystals of nitrite-inhibited FDH_H were obtained by adding 30 mM sodium nitrite to the benzyl viologen solution during oxidation. Diffraction data were processed with DENZO and SCALEPACK (21) or R-AXIS software (22) and scaled with CCP4 programs (23). MIR phases from five derivatives [K₂PtCl₄, Sm(OAc)₃, AuCN, TMLA, and Pb(OAc)₂] together with MAD and anomalous scattering phases (AuCN and TMLA derivatives, respectively) were refined using MLPHARE (23), combined with SIGMAA (23) and subsequently improved through solvent flattening and histogram matching using the program DM (23). The resulting electron density maps were readily interpretable. Model building and refinement were carried out with the programs O (24) and X-PLOR 3.1 (25). The refinement process used all data for which |*I*| > 2 σ _{*I*}. Values of *I*/ σ _{*I*} for the reduced, oxidized, and NO₂⁻-bound data sets were 26.1, 22.1, and 19.5, respectively. During the refinement, ligand bonds to Mo were only loosely restrained (1.0 kcal/Å) and the position of the selenium in reduced FDH_H was fixed.

Data set*	Wave-length (Å)	<i>d</i> _{min} (Å)	Reflections		Completeness (%)	<i>R</i> _{sym} §	Sites (<i>N</i>)	Phasing power
			Measured	Unique				
Native 1	1.5418†	3.0	194,324	17,511	96.0	8.8	—	—
K ₂ PtCl ₄	1.5418†	3.0	188,492	18,059	97.5	11.2	3	0.71
Sm(OAc) ₃	1.5418†	3.0	160,269	16,644	90.3	10.5	2	0.45
AuCN	1.5418†	3.0	161,232	18,353	99.6	10.1	6	0.95
TMLA	1.5418†	3.5	142,691	11,327	95.9	6.1	7	1.29
Pb(OAc) ₂	1.5418†	3.0	183,543	18,514	99.6	8.2	3	0.72
Oxidized	1.5418†	2.8	84,166	20,861	93.4	7.9	—	—
NO ₂ ⁻	1.5418†	2.9	94,068	19,946	97.7	9.0	—	—
Native 2	1.0402‡	2.3	169,244	36,025	88.0	8.5	—	—
AuCNλ1	1.0489‡	3.0	59,714	26,227	75.3	4.3	—	—
AuCNλ2	1.0402‡	3.0	59,419	26,306	75.4	4.3	8	0.64
AuCNλ3	1.0398‡	3.0	51,813	25,231	72.4	4.3	8	0.46
TMLAλ2	0.9493‡	3.0	88,083	29,933	85.7	4.0	8	1.28

FDH model	<i>d</i> spacings (Å)	<i>R</i> value	<i>R</i> _{free}	Non-H atoms (<i>N</i>)	Solvent sites (<i>N</i>)	Mean <i>B</i> factor (Å ²)	rmsd	
							Bonds (Å)	Angles (°)
Reduced	6.0 to 2.3	0.217	0.287	5541	83	28.4	0.013	1.81
Oxidized	6.0 to 2.8	0.195	0.288	5668	64	24.1	0.012	1.81
NO ₂ ⁻ -bound	6.0 to 2.9	0.192	0.282	5671	62	24.1	0.012	1.80

*All data sets were collected at -180°C. AuCN, K₂Au(CN)₂; TMLA, trimethyl lead acetate. †Data collected with an R-AXISIIc system (Molecular Structure Corporation). ‡Data collected at the X4A beamline of the National Synchrotron Light Source (NSLS), Brookhaven, NY. §*R*_{sym} = 100 × $\sum h \sum |I_{h_i} - \langle I_h \rangle| / \sum h \sum I_{h_i}$, where *h* are unique reflection indices, *I*_{*h*} are intensities of symmetry-redundant reflections, and $\langle I_h \rangle$ is the mean intensity. ||Phasing power is the rms value of *F*_{*o*} divided by the rms lack-of-closure error.

REFERENCES AND NOTES

- G. Sawers, *Antonie Leeuwenhoek* **66**, 57 (1994).
- M. J. Axley, D. A. Grahame, T. C. Stadtman, *J. Biol. Chem.* **265**, 18213 (1990).
- M. J. Axley and D. A. Grahame, *ibid.* **266**, 13731 (1991).
- V. N. Gladyshev, S. V. Khangulov, M. J. Axley, T. C. Stadtman, *Proc. Natl. Acad. Sci. U.S.A.* **91**, 7708 (1994).
- M. J. Romão *et al.*, *Science* **270**, 1170 (1995).
- M. K. Chan, S. Mukund, A. Kletzin, M. W. W. Adams, D. C. Rees, *ibid.* **267**, 1463 (1995).
- H. Schindelin, C. Kisker, J. Hilton, K. V. Rajagopalan, D. C. Rees, *ibid.* **272**, 1615 (1996). The overall fold of *Rhodobacter sphaeroides* DMSO reductase is similar to that of FDH_H.
- R. Huber *et al.*, *Proc. Natl. Acad. Sci. U.S.A.* **93**, 8846 (1996).
- T. C. Stadtman, *Annu. Rev. Biochem.* **65**, 83 (1996); R. S. Pilato and E. I. Stiefel, in *Bioinorganic Catalysis*, J. Reedijk, Ed. (Dekker, New York, 1993), chap. 6.
- A. M. Lesk, *Curr. Opin. Struct. Biol.* **5**, 775 (1995); G. E. Schulz, *ibid.* **2**, 61 (1992).
- Sequences were obtained from the SWISS-PROT protein sequence data bank [A. Bairoch and B. Boeckmann, *Nucleic Acids Res.* **20**, 2019 (1992)] (accession numbers p07658, p06131, 032176, p24183, and

- p46448) and the Protein Identification Resource (PIR) [K. E. Sidman, D. G. George, W. C. Barker, L. T. Hunt, *ibid.* **16**, 1869 (1988)] (accession number s18213).
12. The Mo-ligand distances in the reduced form of FDH_H are as follows: MGD⁸⁰¹S12, 2.1 Å; MGD⁸⁰¹S13, 2.3 Å; MGD⁸⁰²S12, 2.5 Å; MGD⁸⁰²S13, 2.3 Å; and Se, 2.5 Å. In the oxidized form of FDH_H, the Mo-ligand distances are as follows: MGD⁸⁰¹S12, 2.6 Å; MGD⁸⁰¹S13, 2.3 Å; MGD⁸⁰²S12, 2.4 Å; MGD⁸⁰²S13, 2.4 Å; Se, 2.7 Å; and OH, 2.2 Å.
 13. M. J. Axley, A. Böck, T. C. Stadtman, *Proc. Natl. Acad. Sci. U.S.A.* **88**, 8450 (1991).
 14. EPR spectroscopy provided evidence that the formate-derived proton is located in the vicinity of the Mo(V) center and is slowly exchangeable with water; the proton-accepting group is weakly involved in the electronic ground state of the Mo(V) center and is not a direct ligand to Mo (S. V. Khangulov, V. N. Gladyshev, T. C. Stadtman, in preparation).
 15. NMR studies of a SeCys²²¹ derivative of subtilisin suggest the presence of a hydrogen bond between the protonated Nε2 of His⁶⁴ and the selenium of SeCys²²¹ [K. L. House, A. R. Garber, R. B. Dunlap, J. D. Odom, D. Hilvert, *Biochemistry* **32**, 3468 (1993)].
 16. S. K. Das, D. Biswas, R. Maiti, S. Sarkar, *J. Am. Chem. Soc.* **118**, 1387 (1996).
 17. G. N. George, J. Hilton, K. V. Rajagopalan, *ibid.*, p. 1113.
 18. M. J. Barber, H. L. May, J. G. Ferry, *Biochemistry* **25**, 8150 (1986).
 19. J. Dong *et al.*, in preparation.
 20. V. N. Gladyshev *et al.*, *J. Biol. Chem.* **271**, 8095 (1996). The results of EPR studies of reduced and oxidized FDH_H crystals are consistent with the presence of a [Mo(IV), Fe₄S_{4(react)}] state and a [Mo(VI), Fe₄S_{4(ox)}] state, respectively.
 21. Z. Otwinowski, in *Proceedings of the CCP4 Study Weekend: Data Collection and Processing*, L. Sawyer, N. Isaacs, S. Bailey, Eds. (SERC Daresbury Laboratory, Warrington, UK, 1993), pp. 56–62.
 22. *R-AxisIIc Data Processing Software Version 2.1 Instruction Manual* (Rigaku Corp., 1994).
 23. *CCP4: A Suite of Programs for Protein Crystallography* (SERC Collaborative Computing Project No. 4, Daresbury Laboratory, Warrington, UK, 1979).
 24. T. A. Jones, J.-Y. Zou, S. W. Cowan, M. Kjeldgaard, *Acta Crystallogr. A* **47**, 110 (1991).
 25. A. T. Brünger, *X-PLOR Version 3.1, a System for X-ray Crystallography and NMR* (Yale Univ. Press, New Haven, CT, 1992).
 26. K. Kraulis, *J. Appl. Crystallogr.* **24**, 946 (1991); D. J. Bacon and W. F. Anderson, *J. Mol. Graphics* **6**, 219 (1988); E. A. Merritt and M. E. P. Murphy, *Acta Crystallogr.* **D50**, 869 (1994).
 27. S. V. Evans, *J. Mol. Graphics* **11**, 134 (1993).
 28. We thank D. A. Grahame for use of the anaerobic glove chamber and helpful discussions, C. Ogata and staff at HHMI beamline X4A, and Y. Zhang and L. Hannick for help in the synchrotron data collection.
- 2 August 1996; accepted 14 January 1997